Configuration mixing of angular-momentum-projected triaxial relativistic mean-field wave functions. II. Microscopic analysis of low-lying states in magnesium isotopes

J. M. Yao,[1] H. Mei,[1] H. Chen,[1] J. Meng,[2,3,4] P. Ring,[5] and D. Vretenar[6]
[1]*School of Physical Science and Technology, Southwest University, Chongqing 400715, China*
[2]*State Key Laboratory of Nuclear Physics and Technology, School of Physics, Peking University, Beijing 100871, China*
[3]*School of Physics and Nuclear Energy Engineering, Beihang University, Beijing 100191, China*
[4]*Department of Physics, University of Stellenbosch, Stellenbosch, South Africa*
[5]*Physik-Department der Technischen Universität München, D-85748 Garching, Germany*
[6]*Physics Department, Faculty of Science, University of Zagreb, HR-10000 Zagreb, Croatia*
(Received 6 June 2010; revised manuscript received 9 December 2010; published 25 January 2011)

The recently developed structure model that uses the generator coordinate method to perform configuration mixing of angular-momentum projected wave functions, generated by constrained self-consistent relativistic mean-field calculations for triaxial shapes (3DAMP+GCM), is applied in a systematic study of ground states and low-energy collective states in the even-even magnesium isotopes $^{20-40}$Mg. Results obtained using a relativistic point-coupling nucleon-nucleon effective interaction in the particle-hole channel and a density-independent δ interaction in the pairing channel are compared to data and with previous axial 1DAMP+GCM calculations, both with a relativistic density functional and the nonrelativistic Gogny force. The effects of the inclusion of triaxial degrees of freedom on the low-energy spectra and $E2$ transitions of magnesium isotopes are examined.

DOI: 10.1103/PhysRevC.83.014308 PACS number(s): 21.10.Ky, 21.10.Re, 21.30.Fe, 21.60.Jz

I. INTRODUCTION

In the first part of this work [1] the simple mean-field (single-reference [2]) implementation of the framework of relativistic energy density functionals (EDF) has been extended to include long-range correlations related to restoration of symmetries broken by the static mean field and to fluctuations of collective coordinates around the mean-field minimum. A model has been developed that uses the generator coordinate method (GCM) to perform configuration mixing of three-dimensional angular-momentum projected (3DAMP) relativistic mean-field wave functions, generated by constrained self-consistent calculations for triaxial nuclear shapes. This calculational framework can be used to perform detailed studies of low-energy collective excitation spectra and corresponding electromagnetic transition rates. The particular implementation of the relativistic 3DAMP+GCM model has been tested in the calculation of spectroscopic properties of low-spin states in ^{24}Mg, in comparison with data and with the results of the recent work of Ref. [3], where a similar 3DAMP+GCM model has been developed, but which was based on nonrelativistic Skyrme triaxial mean-field states that are projected both on particle number and angular momentum and mixed by the GCM. We note that, very recently, a new 3DAMP+GCM model with particle-number projection has been implemented, based on the nonrelativistic Gogny force [4].

In this work we apply the relativistic 3DAMP+GCM model to a systematic study of ground states and low-energy collective states in the even-even magnesium isotopes $^{20-40}$Mg. The low-energy structure of magnesium nuclei has attracted considerable interest in the last decade, both experimental and theoretical. In particular, the sequence of isotopes $^{20-40}$Mg encompasses three spherical magic shell numbers: $N = 8$, 20, and 28 and, therefore, presents an excellent case for studies of the evolution of shell structure with neutron number, weakening of spherical shell closures, disappearance of magic numbers, and the occurrence of "islands of inversion" [5]. Following the pioneering measurement of the transition rate $B(E2; 0_1^+ \rightarrow 2_1^+)$ in the neutron-rich nucleus ^{32}Mg [6] that confirmed a large deformation of this nucleus indicated by the low excitation energy of the 2_1^+ state [7], extensive experimental studies of the low-energy structure of Mg isotopes have been carried out at the Institute of Physical and Chemical Research, Japan (RIKEN) [8,9], Michigan State University (MSU) [10–13], the Grand Accélérateur National d'Ions Lourds, France (GANIL) [14] and CERN [15,16].

In addition to numerous theoretical studies based on large-scale shell-model calculations [17–22], the self-consistent mean-field framework, including the nonrelativistic Hartree-Fock-Bogolibov (HFB) model with Skyrme [23] and Gogny forces [24] and the relativistic mean-field (RMF) model [25,26] as well as the macroscopic-microscopic model based on a modified Nilsson potential [27], have been used to analyze the ground-state properties (binding energies, charge radii, and deformations) and low-lying excitation spectra of magnesium isotopes. Of course, to calculate excitation spectra and electromagnetic transition rates, in particular for transitional nuclei, it is necessary to go beyond the mean-field approximation and include dynamic correlations related to the restoration of broken symmetries and to fluctuations of collective coordinates. Based on the 1DAMP+GCM (axial symmetry) framework, studies of low-energy spectra of specific Mg isotopes have been performed using nonrelativistic models with Skyrme [28,29] and Gogny [24] forces, as well as relativistic density functionals [30,31].

In Sec. II we present a brief outline of the relativistic 3DAMP+GCM model used in the present analysis. Section III describes a study of low-lying collective states of the even-even

magnesium isotopes $^{20-40}$Mg. A brief summary and an outlook for future studies are included in Sec. IV.

II. THE 3DAMP+GCM MODEL

The 1DAMP+GCM calculational framework, restricted to axially symmetric nuclei, has recently been extended to include triaxial shapes. 3DAMP+GCM models have been developed based on the self-consistent Hartree-Fock-Bogoliubov approach with Skyrme forces [3] and the Gogny force [4]. Starting from relativistic energy density functionals, we have implemented a model for configuration mixing of three-dimensional angular-momentum projected (3DAMP) relativistic mean-field wave functions, generated by constrained self-consistent calculations for triaxial nuclear shapes. The details of the model and the numerical tests are described in Refs. [1,32]. Here we only outline the basic features of the model that will be used in the study of low-lying states in even-even magnesium isotopes $^{20-40}$Mg.

In the 3DAMP+GCM framework the trial angular-momentum projected GCM collective wave function $|\Psi_\alpha^{JM}\rangle$, an eigenfunction of $\hat{J}^2$ and $\hat{J}_z$ with eigenvalue $J(J+1)\hbar^2$ and $M\hbar$, respectively, reads

$$\left|\Psi_\alpha^{JM}\right\rangle = \int d^2q \sum_{K\geqslant 0} f_\alpha^{JK}(q)\frac{1}{(1+\delta_{K0})}|JMK+,q\rangle, \qquad (1)$$

where $\alpha = 1, 2, \ldots$ labels collective eigenstates for a given angular momentum J, and q is the generic notation for the deformation parameters β and γ. The basis states $|JMK+,q\rangle$ are projected from the intrinsic wave functions $|\Phi(q)\rangle$:

$$|JMK+,q\rangle = \left[\hat{P}^J_{MK} + (-1)^J \hat{P}^J_{M-K}\right]|\Phi(q)\rangle, \qquad (2)$$

where $\hat{P}^J_{MK}$ denotes the angular-momentum projection operator:

$$\hat{P}^J_{MK} = \frac{2J+1}{8\pi^2}\int d\Omega D^{J*}_{MK}(\Omega)\hat{R}(\Omega). \qquad (3)$$

Ω denotes the set of three Euler angles $\{\phi,\theta,\psi\}$ and $d\Omega = d\phi\sin\theta d\theta d\psi$. $D^J_{MK}(\Omega)$ is the Wigner D function, and the rotational operator reads $\hat{R}(\Omega) = e^{i\phi\hat{J}_z}e^{i\theta\hat{J}_y}e^{i\psi\hat{J}_z}$. The set of deformed intrinsic wave functions $|\Phi(q)\rangle$ is generated by imposing constraints on the axial q_{20} and triaxial q_{22} mass quadrupole moments in self-consistent RMF+BCS calculations.

The weight functions $f_\alpha^{JK}(q)$ in the collective wave function Eq. (1) are obtained from the solution of the Hill-Wheeler-Griffin (HWG) integral equation:

$$\int dq' \sum_{K'\geqslant 0}\left[\mathscr{H}^J_{KK'}(q,q') - E^J_\alpha \mathscr{N}^J_{KK'}(q,q')\right]f_\alpha^{JK'}(q') = 0, \qquad (4)$$

where $\mathscr{H}$ and $\mathscr{N}$ are the angular-momentum projected GCM kernel matrices of the Hamiltonian and the norm, respectively [1].

The basis states $|JMK+,q\rangle$ in Eq. (1) are not eigenstates of the proton and neutron number operators $\hat{Z}$ and $\hat{N}$. In order to approximately restore the correct mean values of the nucleon numbers, we follow the prescription given in Refs. [33,34]. The validity of such a correction scheme is discussed in Appendix.

The solution of Eq. (4) determines both the energies E^J_α and the amplitudes $f_\alpha^{JK}(q)$ of collective states $|\Psi_\alpha^{JM}\rangle$ with good angular momentum. The center-of-mass correction to the total energy of the state J^π_α is calculated in the zeroth order of the Kamlah approximation.

Since the weight functions $f_\alpha^{JK}(q)$ are not orthogonal and cannot be interpreted as collective wave functions for the deformation variables, the collective wave functions $g^J_\alpha(i)$ are determined from the eigenstates of the norm overlap kernel

$$g^J_\alpha(i) = \sum_k g_k^{J\alpha}u_k^J(i). \qquad (5)$$

These functions are orthonormal and

$$\sum_i \left|g^J_\alpha(i)\right|^2 = 1, \qquad (6)$$

where the sum is over $i \equiv \{K,q\}$. The coefficients $g_k^{J\alpha}$ are solutions of the following equation:

$$\sum_l \mathcal{H}^J_{kl}g_l^{J\alpha} = E^J_\alpha g_k^{J\alpha}, \qquad (7)$$

which is equivalent to Eq. (4). The matrix $\mathcal{H}^J_{kl}$ is determined by the angular-momentum projected GCM kernel matrix of the Hamiltonian

$$\mathcal{H}^J_{kl} = \frac{1}{\sqrt{n^J_k}}\frac{1}{\sqrt{n^J_l}}\sum_{i,j}u^J_k(i)\mathscr{H}^J(i,j)u^J_l(j), \qquad (8)$$

where n^J_k and u^J_k are the nonvanishing eigenvalues and eigenvectors of the norm overlap kernel $\mathscr{N}^J(i,j)$, respectively.

The $B(E2)$ value for a transition from an initial state (J_i,α_i) to a final state (J_f,α_f) is calculated from

$$B(E2;J_i,\alpha_i\rightarrow J_f,\alpha_f) = \frac{e^2}{2J_i+1}|\langle J_f,\alpha_f||\hat{Q}_2||J_i,\alpha_i\rangle|^2, \qquad (9)$$

where the reduced matrix element is defined by

$$\begin{aligned}&\langle J_f,\alpha_f||\hat{Q}_2||J_i,\alpha_i\rangle \\ &= \sum_{ij}(2J_f+1)\sum_{K_iK_f}f^{*J_fK_f}_{\alpha_f}(q_i)f^{J_iK_i}_{\alpha_i}(q_j)\sum_{\mu K'}(-1)^{J_f-K_f} \\ &\times\begin{pmatrix}J_f & 2 & J_i\\ -K_f & \mu & K'\end{pmatrix}\langle\Phi(q_i)|\hat{Q}_{2\mu}\hat{P}^{J_i}_{K'K_i}|\Phi(q_j)\rangle, \end{aligned} \qquad (10)$$

with $f_\alpha^{JK}(q) = (-1)^J f_\alpha^{J-K}(q)$ for $K<0$. The spectroscopic quadrupole moment for the state (J^π_α) is defined by the expression

$$\begin{aligned}Q^{\rm spec}(J^\pi_\alpha) &= e\sqrt{\frac{16\pi}{5}}\langle J,M=J,\alpha|\hat{Q}_{20}|J,M=J,\alpha\rangle \\ &= e\sqrt{\frac{16\pi}{5}}\begin{pmatrix}J & 2 & J\\ J & 0 & -J\end{pmatrix}\langle J,\alpha||\hat{Q}_2||J,\alpha\rangle. \end{aligned} \qquad (11)$$

The matrix elements of the charge quadrupole operator $\hat{Q}_{2\mu} = e\sum_p r_p^2Y_{2\mu}(\Omega_p)$ are calculated in the full configuration

space. There is no need for effective charges, and e simply corresponds to the bare value of the proton charge.

III. LOW-LYING STATES IN MAGNESIUM ISOTOPES: RESULTS AND DISCUSSION

As in the first part of this work [1], we use the relativistic point-coupling interaction PC-F1 [35] in the particle-hole channel, and the corresponding density-independent δ force in the particle-particle channel. The parameters of the PC-F1 functional and the pairing strength constants V_n and V_p have been adjusted simultaneously to the nuclear matter equation of state, and to ground-state observables (binding energies, charge and diffraction radii, surface thickness, and pairing gaps) of spherical nuclei [35], with pairing correlations treated in the BCS approximation. In particular, the pairing strength parameters for neutrons and protons are $V_n = -308$ MeV fm^3 and $V_p = -321$ MeV fm^3, respectively.

Parity, D_2 symmetry, and time-reversal invariance are imposed in the constrained mean-field calculation of the binding energy map of a (generally) triaxial, even-even nucleus. To solve the Dirac equation for triaxially deformed potentials, the single-nucleon spinors are expanded in the basis of eigenfunctions of a three-dimensional harmonic oscillator (HO) in Cartesian coordinates, with $N_{\rm sh} = 8$ major shells for $^{20-26}$Mg and $N_{\rm sh} = 10$ for $^{28-40}$Mg. These numbers of oscillator shells are sufficient to obtain a reasonably converged mean-field potential energy surface [1,32]. The HO basis is chosen to be isotropic; that is, the oscillator parameters $b_x = b_y = b_z = b_0 = \sqrt{\hbar/m\omega_0}$ in order to keep the basis closed under rotations [36,37]. The oscillator frequency is given by $\hbar\omega_0 = 41A^{-1/3}$. The Gaussian-Legendre quadrature is used for integrals over the Euler angles ϕ, θ, and ψ in the calculation of the norm and hamiltonian kernels. As illustrated in Ref. [32] that, with the choice of the number of mesh points for the Euler angles (ϕ, θ, ψ) in the interval $[0, \pi]$ being $N_\phi = N_\psi = 8$ and $N_\theta = 12$, the calculation could achieve an accuracy of $\approx$0.05% for the energy of a projected state with angular momentum $J \leqslant 6$ in the ground-state band. In the 3DAMP+GCM calculations of ^{24}Mg it has been shown that, because of very few level crossings as a function of deformation, redundancies appear very quickly in the norm kernel when more states are added to the nonorthogonal basis [1,3]. The generator coordinates are, therefore, chosen in the intervals $0 \leqslant \beta \leqslant 1.2$ and $0 \leqslant \gamma \leqslant 60^\circ$, with steps $\Delta\beta = 0.2$ and $\Delta\gamma = 20^\circ$, respectively. Moreover, eigenstates of the norm overlap kernel with very small eigenvalues $n_k^J/n_{\rm max}^J < \zeta$ are removed from the GCM basis. With the cutoff parameter $\zeta = 5 \times 10^{-3}$ for $^{20-26}$Mg and $\zeta = 1 \times 10^{-4}$ for $^{28-40}$Mg, fully converged results are obtained for all low-lying states with $J < 6$.

In Fig. 1 we plot the self-consistent RMF+BCS mean-field, and the corresponding angular-momentum projected $(J^\pi = 0^+)$ energy curves (PEC) for the even-even magnesium isotopes $^{20-40}$Mg, as functions of the axial deformation β $(\gamma = 0)$. One might notice an interesting evolution of the mean-field PECs from a spherical shape at magic neutron number $N = 8$, through pronounced prolate shapes, coexistence of oblate and prolate shapes, and again to a spherical shape at $N = 20$. Increasing further the neutron number from $N = 20$ to $N = 28$, the mean-field minima become markedly prolate. Furthermore, the effect of angular-momentum projection can be inferred from a comparison with the corresponding $(J^\pi = 0^+)$ PECs in the right panel of Fig. 1. In particular, in the neighborhood of the spherical minimum, the $J = 0$ PECs of ^{20,32}Mg are very soft with respect to β. In other isotopes the deformed minima become deeper after projection.

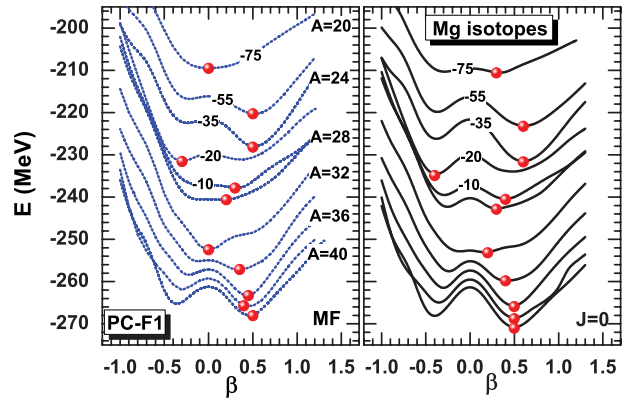

FIG. 1. (Color online) Self-consistent RMF+BCS mean-field (left panel), and angular-momentum projected 0^+ potential energy curves (PEC, right panel) of even-even magnesium isotopes, as functions of the axial deformation parameter β. To plot all the curves in the same figure, the PECs of $^{20-28}$Mg have been shifted by -75, -55, -35, -20, and -10 MeV, respectively. The position of the minimum of each PEC is indicated by a red dot.

Figure 2 displays the total ground-state dynamical correlation energies of Mg isotopes as a function of the number of neutrons. As shown in the figure, $E_{\rm Corr}$ consists of a rotational energy correction $\Delta E_{J=0}$ that results from the restoration of rotational symmetry

$$\Delta E_{J=0} = E_{J=0}(\beta_0) - E_{\rm MF}(\beta_m) \tag{12}$$

and the correlation energy gained by GCM configuration mixing

$$\Delta E_{\rm GCM} = E(0_1^+) - E_{J=0}(\beta_0). \tag{13}$$

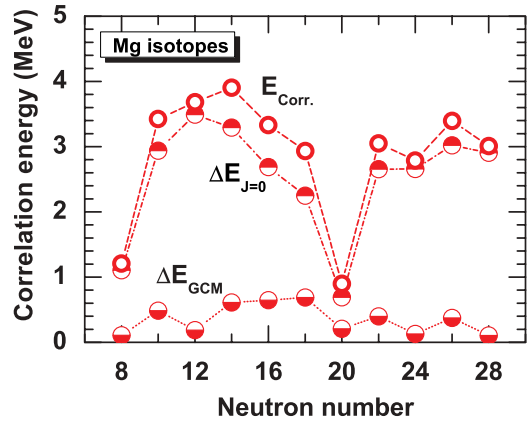

FIG. 2. (Color online) Total ground-state dynamical correlation energies $E_{\rm Corr}$ of Mg isotopes as a function of the number of neutrons. $E_{\rm Corr}$ is the sum of the rotational energy correction $\Delta E_{J=0}$ and the energy gained by configuration mixing, $\Delta E_{\rm GCM}$.

β_m and β_0 denote the axial deformation parameters at the minima of the mean field and the ($J^\pi = 0^+$) angular-momentum projected PECs, respectively (cf. Fig. 1). $E_{\rm Corr}$ shows a strong dependence on shape and shell structure. It is large for deformed midshell nuclei, with a maximum of ~4 MeV at $N = 14$, and is drastically reduced (~1 MeV) for the two isotopes with the neutron magic numbers $N = 8$ and $N = 20$. Projection on angular momentum $J = 0$; that is, the rotational energy correction $\Delta E_{J=0}$, constitutes the dominant part of the total dynamical correlation energy. This is generally valid for a great majority of nuclei, as it has been shown in the global study of quadrupole correlation effects [39] performed with GCM configuration mixing of axially symmetric Skyrme-Hartree-Fock+BCS states, with the two-point topological Gaussian overlap approximation for angular-momentum projection. As also shown in Ref. [39], in Fig. 2 one notices that the correlation energy $\Delta E_{\rm GCM}$ gained from configuration mixing of different deformed states is of the order of several hundreds of keV, and not very sensitive to nuclear shape and shell structure. $\Delta E_{\rm GCM}$ is, in fact, composed of two parts: a potential term that is negative and comparable in size to the correlation energy induced by angular-momentum projection, and a kinetic part (energy of the zero-point vibrational motion) that is positive and cancels to a large extent the potential term [40].

The excitation energies of the states 2_1^+ and 4_1^+ in $^{20-40}$Mg, calculated using the 1DAMP+GCM model with the relativistic density functional PC-F1, are compared in Fig. 3 to the available data and the prediction of the 1DAMP+GCM calculation based on the nonrelativistic HFB framework with the Gogny force [24]. Both models yield excitation energies of the 2_1^+ and 4_1^+ states in reasonable agreement with data and, on average, the values obtained with PC-F1 are 10%–30% lower than those calculated with the Gogny interaction D1S

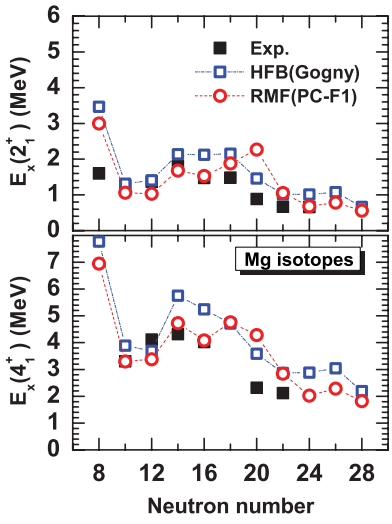

FIG. 3. (Color online) Excitation energies of the states 2_1^+ and 4_1^+ in $^{20-40}$Mg, calculated using the 1DAMP+GCM model with the relativistic density functional PC-F1, are compared to available data [12,13,38] and the results of the 1DAMP+GCM calculation based on the nonrelativistic HFB framework with the Gogny force [24].

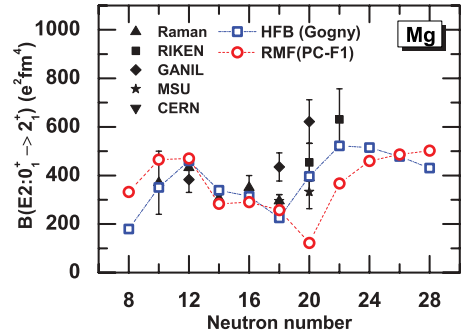

FIG. 4. (Color online) $B(E2; 0_1^+ \to 2_1^+)$ (e^2fm^4) values in $^{20-40}$Mg, calculated using the 1DAMP+GCM model with the relativistic density functional PC-F1, are compared to available data [6,8,10,14,15,38] and the results of the 1DAMP+GCM calculation based on the nonrelativistic HFB framework with the Gogny force [24].

(except for ^{32}Mg). This is due to relatively weak neutron pairing correlations in the present calculation that lead to an increase of the corresponding moment of inertia for the yrast states. As noted in our previous study of ^{24}Mg in Ref. [1], the excitation energies of yrast states increase when the pairing strength parameters V_n or V_p are adjusted to the pairing gaps determined from empirical odd-even mass differences in this particular mass region. Both calculations preserve the $N = 8$ magic number and, with PC-F1 also at $N = 20$, a pronounced shell closure is obtained, whereas the model based on the Gogny force predicts a much lower excitation energy of the 2_1^+ state in ^{32}Mg, in better agreement with data. One might notice, however, that both models predict the 4_1^+ state in this nucleus at energies far above the experimental value. The $N = 28$ shell closure disappears in both calculations, and ^{40}Mg is predicted to be prolate deformed.

The corresponding $B(E2; 0_1^+ \to 2_1^+)$ (e^2fm^4) values in $^{20-40}$Mg are shown in Fig. 4. The 1DAMP+GCM calculations, both the present one using the functional PC-F1 and that based on the Gogny force [24], yield results in reasonable agreement with data except, of course, PC-F1 at and in the neighborhood of neutron number $N = 20$. Since the Gogny force D1S predicts an axially deformed ground state for ^{32}Mg, the corresponding $B(E2)$ value for the transition $0_1^+ \to 2_1^+$ is much closer to the experimental value, compared to the calculation with PC-F1, which yields a spherical ground state at $N = 20$. The functional PC-F1, together with the density-independent δ force ($V_n = -308$ MeV fm^3 and $V_p = -321$ MeV fm^3) predicts indeed a very small $B(E2)$ value for this transition in ^{32}Mg. In Ref. [32] it has been suggested that a better adjustment of pairing strength parameters and, eventually, the inclusion of triaxiality (i.e., the γ degree of freedom), could improve the results for ^{32}Mg. Already in the 1DAMP+GCM axial calculations we have verified that, by adjusting the pairing strengths specifically to the empirical pairing gaps around ^{32}Mg (five-point formula) of $V_n = -465$ MeV fm^3 and $V_p = -350$ MeV fm^3, the calculated transition rate increases to $B(E2; 0_1^+ \to 2_1^+) = 313.5$ e^2fm^4. To have a consistent model, however, in the remaining calculations of this work we will continue using the original pairing strengths

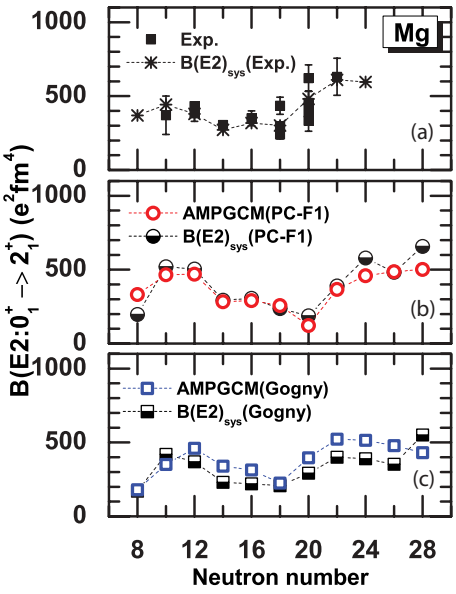

FIG. 5. (Color online) $B(E2)$ values calculated with the LDM formula Eq. (14) for the transition $0_1^+ \to 2_1^+$ in Mg isotopes, are compared to data [6,8,10,14,15,38] in panel (a), and to the results of the 1DAMP+GCM calculations with the functional PC-F1 in (b), and with the Gogny force D1S [24] in (c).

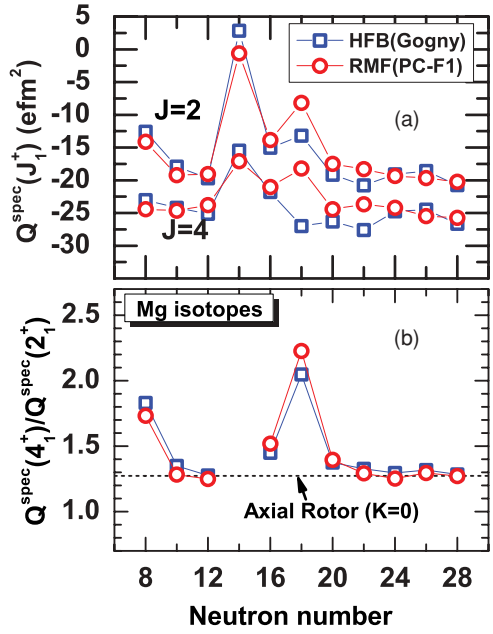

FIG. 6. (Color online) Spectroscopic quadrupole moments of the states 2_1^+ and 4_1^+ in $^{20-40}$Mg, calculated using the 1DAMP+GCM model with the relativistic density functional PC-F1, and the corresponding values based on the nonrelativistic HFB framework with the Gogny force [24] (upper panel). The calculated ratios $Q^{\rm spec}(4_1^+)/Q^{\rm spec}(2_1^+)$ are compared to the value that corresponds to a rigid axial rotor with $K = 0$ (lower panel).

that were adjusted simultaneously with the parameters of the PC-F1 effective interaction in the particle-hole channel [35].

An empirical formula based on the liquid-drop model (LDM) provides us a useful guideline to examine the nuclear collectivity [41],

$$B(E2: 0_1^+ \to 2_1^+)_{\rm sys} = 5 \times 6.47 Z^2 A^{-0.69} E_x^{-1}(2_1^+). \qquad (14)$$

It has been noted in Ref. [41] that, for open-shell nuclei, the ratio $B(E2: 0_1^+ \to 2_1^+)_{\rm expt}/B(E2: 0_1^+ \to 2_1^+)_{\rm sys}$ is mostly around 1.0, being confined between 0.5 and 2.0. For the closed-shell nuclei, the ratio is also often larger than 0.20. Therefore, the significant deviation of the ratio from these values can be a signature of existence of anomalous collectivity, as found in ^{16}C [42]. In order to examine the collectivity in magnesium isotopes, we make a comparison of the experimental and calculated $B(E2; 0_1^+ \to 2_1^+)$ with the prediction of the LDM expression. This comparison is shown in Fig. 5. In the upper panel the $B(E2)$ values calculated with the LDM formula are compared to data, whereas in the two lower panels they are compared to the results of the 1DAMP+GCM calculations with the functional PC-F1 and with the Gogny force D1S. The excitation energies $E(2_1^+)$ (in MeV) that appear in the LDM expression Eq. (14), correspond to the experimental values and those calculated with PC-F1 and Gogny D1S, respectively. One notices a very good agreement between data and the $B(E2)$ values predicted by the LDM formula. Based on the recently measured $E(2_1^+)$ values for ^{20}Mg [1598 (10) keV] and ^{36}Mg [660 (6) keV], Eq. (14) predicts the corresponding $B(E2; 0_1^+ \to 2_1^+)$ values of 368.9 (23) e^{2}fm^4 and 595.4 (54) e^{2}fm^4, respectively. The 1DAMP+GCM calculation based on the PC-F1 functional yields somewhat smaller $B(E2)$ values for the $0_1^+ \to 2_1^+$ transition in ^{20}Mg (332 e^{2}fm^4) and ^{36}Mg (460 e^{2}fm^4).

In Fig. 6 we plot the spectroscopic quadrupole moments of the states 2_1^+ and 4_1^+ in $^{20-40}$Mg, calculated using the 1DAMP+GCM model with the relativistic density functional PC-F1 and compared to the corresponding values based on the nonrelativistic HFB framework with the Gogny force [24]. One might notice a very good agreement between the results of the two model calculations, with the exception of ^{30}Mg. In the lower panel the calculated ratios $Q^{\rm spec}(4_1^+)/Q^{\rm spec}(2_1^+)$ are compared to the value that corresponds to a rigid axial rotor with $K = 0$ (i.e., $\approx$1.27). In ^{26}Mg both models predict a very small value of $Q^{\rm spec}(2_1^+)$, and this gives rise to an exceptionally high value of $Q^{\rm spec}(4_1^+)/Q^{\rm spec}(2_1^+)$ that does not fit the scale of the vertical axis. This result indicates that there is a large contribution from nonzero-K components in the yrast band of ^{26}Mg. Large deviations from the axial rotor value are also predicted for ^{20}Mg and ^{30}Mg. For the isotopes $^{22,24,28,32-40}$Mg both models yield $Q^{\rm spec}(4_1^+)/Q^{\rm spec}(2_1^+)$ quite close to that of rigid axial rotor. Note that this is also true in ^{32}Mg, for which the calculation based on the Gogny force yields a deformed ground state, whereas this state is spherical in the present axially symmetric calculation using the functional PC-F1. In both calculations, however, the states 2_1^+ and 4_1^+ are prolate deformed.

To examine the influence of triaxiality i.e., of including the γ degree of freedom) on the spectroscopic properties of low-lying states in magnesium isotopes, we have performed full 3DAMP+GCM calculations using the relativistic functional PC-F1. In Figs. 7 and 8 we display the resulting self-consistent RMF+BCS triaxial quadrupole binding energy maps of the even-even $^{20-40}$Mg isotopes in the β-γ plane ($0 \leqslant \gamma \leqslant 60^0$),

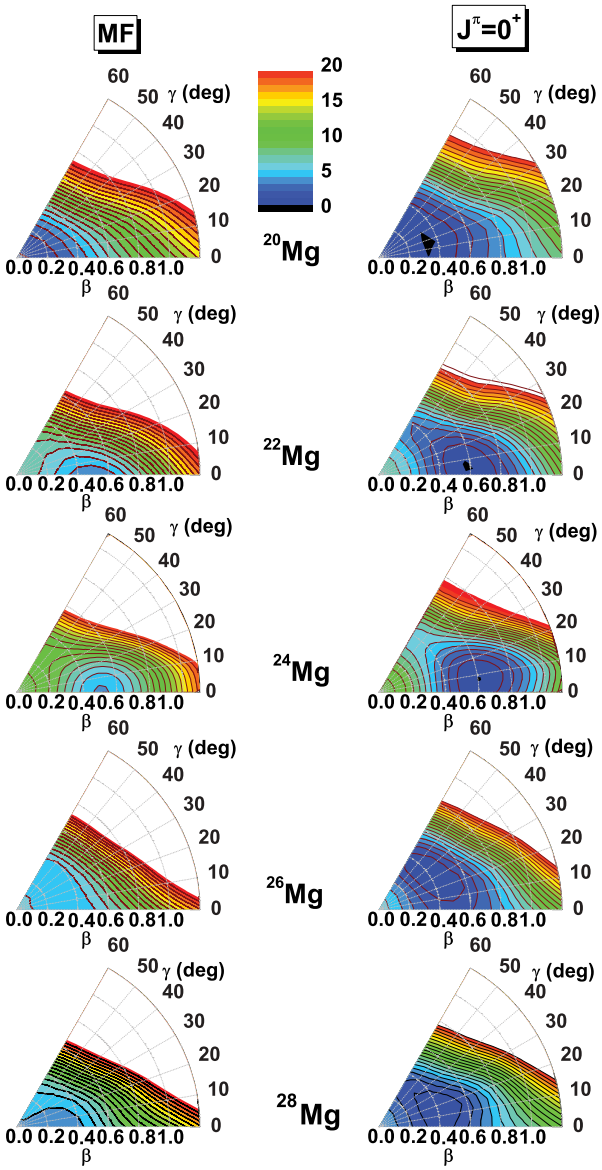

FIG. 7. (Color online) Self-consistent RMF+BCS triaxial quadrupole binding energy maps of the even-even $^{20-28}$Mg isotopes in the β-γ plane ($0 \leqslant \gamma \leqslant 60^\circ$, left panel), and the corresponding angular-momentum $J^\pi = 0^+$ projected energy surfaces (right panel). All energies are normalized with respect to the binding energy of the absolute minimum, and the contours join points on the surface with the same energy (in MeV).

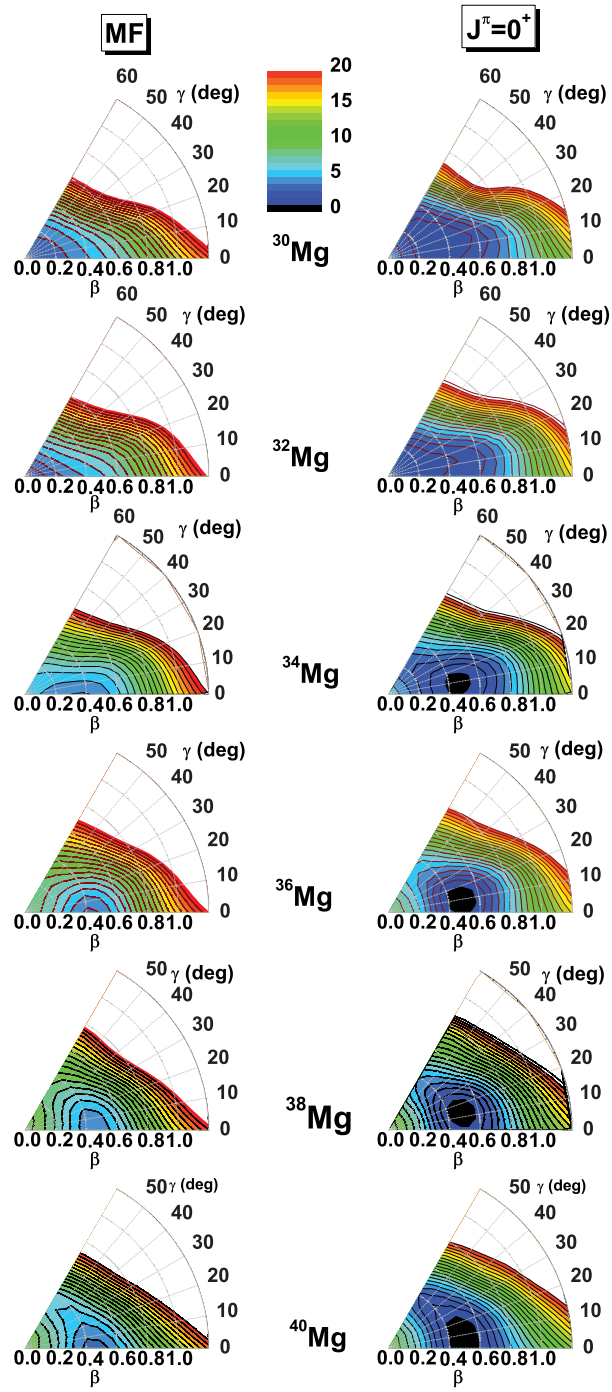

FIG. 8. (Color online) Same as described in the caption to Fig. 7 but for the isotopes $^{30-40}$Mg.

and the corresponding angular-momentum $J^\pi = 0^+$ projected energy surfaces. All energies are normalized with respect to the binding energy of the absolute minimum, the contours join points on the surface with the same energy (in MeV). In general, the inclusion of the triaxial deformation degree of freedom reduces considerably the barriers separating axially prolate and oblate minima in the well-deformed isotopes $^{22,24,34-40}$Mg. We also notice that the angular-momentum $J^\pi = 0^+$ projected energy surfaces of $^{26-32}$Mg are rather soft both in β and γ.

The low-energy excitation spectra and collective wave functions are calculated as solutions of the Hill-Wheeler-Griffin integral equation for each angular momentum, and thus take into account fluctuations of the collective coordinates β and γ around the mean-field minima. For the sequence of isotopes $^{20-40}$Mg, Figs. 9 and 10 display the probability distributions $|g_\alpha^J|^2$ of the collective wave functions Eq. (5) in the β-γ plane for the states 0_1^+ and 2_1^+ (both the $K = 0$ and $K = 2$ components). It appears that ^{20,30,32}Mg are spherical in the ground state, whereas all the other isotopes are prolate deformed and the ground-state deformation is especially

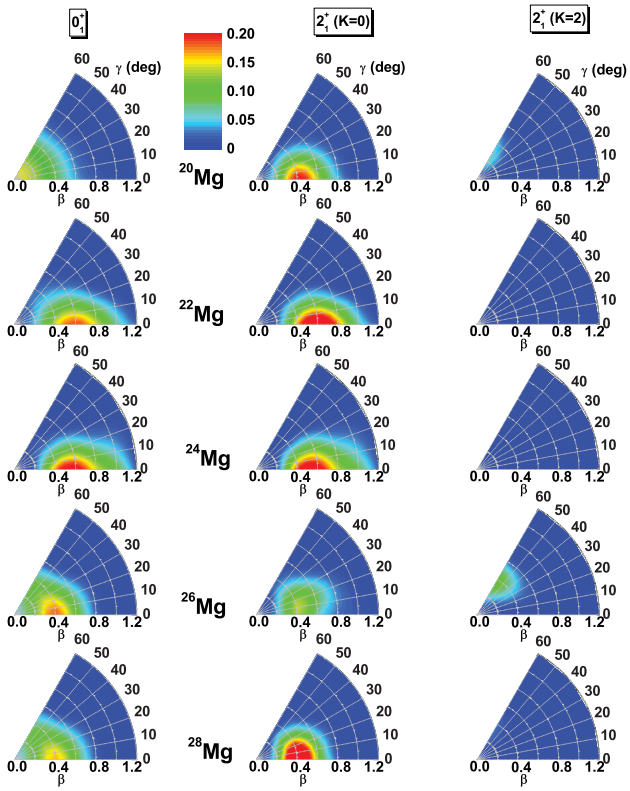

FIG. 9. (Color online) Probability distributions $|g_\alpha^J|^2$ of the collective wave functions Eq. (5) in the β-γ plane, for the states of 0_1^+ and 2_1^+ (both the $K = 0$ and $K = 2$ components) of $^{20-28}$Mg.

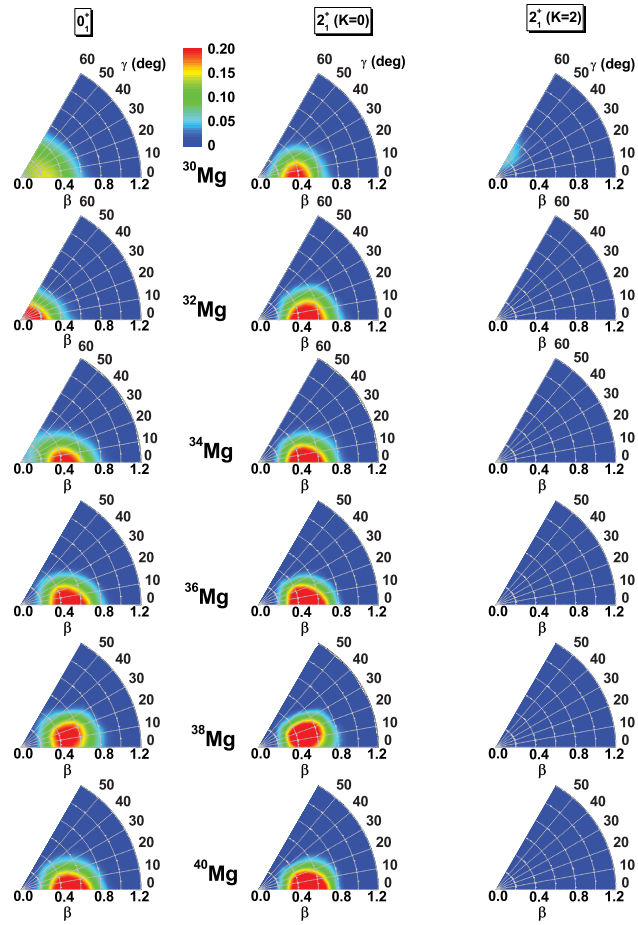

FIG. 10. (Color online) Same as described in the caption to Fig. 9, but for the isotopes $^{30-40}$Mg.

pronounced in heavier Mg nuclei. The first excited state 2_1^+ is prolate deformed in all Mg nuclei, even in ^{32}Mg. In several isotopes, most notably in ^{26}Mg and ^{30}Mg, the collective wave function of the state 2_1^+ contains sizable admixtures of the $K = 2$ component. This can be seen more clearly in Fig. 11 where, after integrating the probability distributions over β and γ, we plot in the upper panel the relative weight of the $K = 0$ component in the collective wave functions of the 2_1^+ states of magnesium isotopes $^{20-40}$Mg. The softness toward triaxial shapes is especially pronounced in ^{20}Mg, ^{26}Mg, and ^{30}Mg. The contribution of the $K = 2$ component in the wave functions of 2_1^+ will generally affect the calculated $B(E2)$ values for transitions to the ground state. In the lower panel of Fig. 11 we show the differences between the $B(E2; 2_1^+ \to 0_1^+)$ values calculated in the full 3DAMP+GCM and the axial 1DAMP+GCM models, normalized to the 1D values. A marked effect of K mixing is found not only in ^{26}Mg, but also in some heavier isotopes including ^{32}Mg.

Finally, a quantitative comparison between the axial 1DAMP+GCM and the full 3DAMP+GCM calculations for $^{20-40}$Mg, based on the relativistic functional PC-F1, is presented in Table I. The ground-state energies $E_{\rm gs}$ (in MeV), excitation energies of the 2_1^+ and 4_1^+ states (in MeV), and $B(E2\downarrow; J \to J-2)$ values (in e^2fm^4) for the lowest states with $J = 2^+$ and 4^+ in magnesium isotopes are included in the table. In general, the inclusion of the γ degree of freedom leads to the lowering of the binding energies of low-lying states and to an increase of the calculated $B(E2)$ values. The latter is particularly prominent in ^{26}Mg, in which the 3DAMP+GCM yields an enhancement of ≈25% for the $B(E2; 0_1^+ \to 2_1^+)$. Especially interesting is the case of ^{32}Mg, which shows a pronounced lowering of the excitation energies of 2_1^+ and 4_1^+, whereas the binding energy of the ground state, being spherical, is not influenced by the inclusion of triaxial shapes. These excitation energies are, however, still far above the experimental energies and, although the $B(E2; 0_1^+ \to 2_1^+)$ value increases by ≈10%, it is about a factor three smaller than the empirical value. However, when the pairing strength parameters are adjusted specifically to the empirical pairing gaps around ^{32}Mg (five-point formula) of $V_n = -465$ MeV fm^3 and $V_p = -350$ MeV fm^3, the calculated transition rate increases to $B(E2; 0_1^+ \to 2_1^+) = 330.1$ e^{2}fm^4, in rather good agreement with data. This results shows the importance of a more detailed study of pairing correlations in $N \approx 20$ neutron-rich nuclei.

IV. SUMMARY

The very successful framework of relativistic energy density functionals has mostly been used on the mean-field level to describe ground-state properties of medium-heavy and heavy nuclei. When considering applications, however, it is important to develop EDF-based structure models that

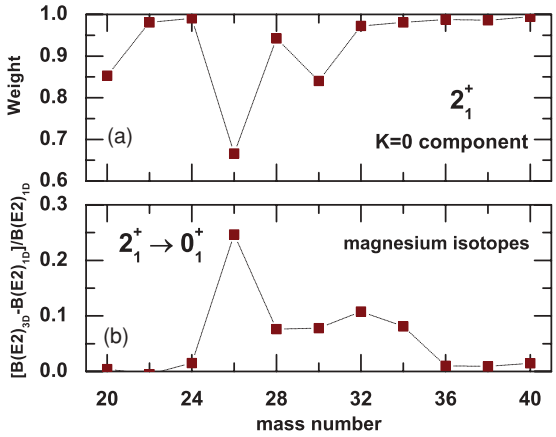

FIG. 11. (Color online) Upper panel shows the relative weight of the $K = 0$ component in the collective wave functions of the 2_1^+ states of magnesium isotopes $^{20-40}$Mg. Lower panel shows the differences between the $B(E2; 2_1^+ \rightarrow 0_1^+)$ values calculated in the 3DAMP+GCM and the 1DAMP+GCM models, normalized to the 1D values.

go beyond the static mean-field approximation. Detailed predictions of excitation spectra and transition rates necessitate the inclusion of correlations related to the restoration of broken symmetries and to fluctuations of collective variables. In recent years, several new models have been developed that extend the relativistic EDF-based approach and perform the restoration of symmetries broken by the static mean field and take into account fluctuations around the mean-field minimum. This is relatively simple in the case of axial symmetry; that is, when only one collective coordinate is considered [30,31], but such models become much more involved, technically complicated, and computationally demanding when possible triaxial shapes are taken into account.

In Refs. [32] and [1] we have implemented and tested a new model that uses the generator coordinate method (GCM) to perform configuration mixing of three-dimensional angular-momentum projected (3DAMP) relativistic mean-field wave functions, generated by constrained self-consistent calculations for triaxial nuclear shapes. In the present study this calculational framework has been used to analyze the influence of triaxiality on the low-energy collective excitation spectra and the corresponding electric quadrupole transition rates of even-even magnesium isotopes $^{20-40}$Mg. The self-consistent solutions of the constrained RMF+BCS equations have been obtained using the relativistic point-coupling interaction PC-F1 [35] in the particle-hole channel, and a density-independent δ force in the particle-particle channel. Since the low-energy spectra of $^{20-40}$Mg were previously investigated in the axial 1DAMP+GCM model based on the nonrelativistic HFB framework with the Gogny force [24], in the first instance we have performed axial 1D calculations and compared the results with data and those obtained in Ref. [24]. In general, a good agreement has been obtained between the results of the two model calculations, except for ^{30,32}Mg. The low excitation energy of 2_1^+ and the large $B(E2; 0_1^+ \rightarrow 2_1^+)$ indicate that the neutron rich nucleus ^{32}Mg is deformed, even though the number of neutrons equal the "spherical magic number" $N = 20$. The data are reproduced reasonably well by the 1DAMP+GCM model based on the Gogny force, which yields a deformed ground state for ^{32}Mg. The present axial calculation, on the other hand, predicts a spherical β-soft ground state for ^{32}Mg, although the lowest excited states 2_1^+ and 4_1^+ are calculated to be prolate deformed. The corresponding $B(E2; 0_1^+ \rightarrow 2_1^+)$ is much smaller than the experimental value. Both models predict prolate ground states for heavier Mg isotopes, including the $N = 28$ nucleus ^{40}Mg.

To analyze the effect of triaxiality and K-mixing on the low-energy structure of Mg isotopes, we have also performed a full 3DAMP+GCM calculation based on the relativistic density functional PC-F1 and a density-independent δ pairing interaction. When compared with the 1DAMP+GCM results, it is noted that the inclusion of the γ degree of freedom leads to the lowering of the binding energies of low-lying states and to an increase of the calculated $B(E2)$ values in deformed isotopes. In several isotopes, a pronounced degree of γ softness and K mixing is predicted for the yrast states. The

TABLE I. The ground-state energy E_{gs} (in MeV), excitation energies of the 2_1^+ and 4_1^+ states (in MeV), and $B(E2\uparrow; J-2 \rightarrow J)$ values (in e^2fm^4) for the lowest states with $J = 2^+$ and 4^+ in magnesium isotopes. Results obtained in the axial 1DAMP+GCM calculation are compared with those of the full 3DAMP+GCM model.

	1DAMP+GCM					3DAMP+GCM				
Isotopes	E_{gs}	$E_x(2_1^+)$	$E_x(4_1^+)$	$E2\uparrow(2_1^+)$	$E2\uparrow(4_1^+)$	E_{gs}	$E_x(2_1^+)$	$E_x(4_1^+)$	$E2\uparrow(2_1^+)$	$E2\uparrow(4_1^+)$
^{20}Mg	−135.501	2.999	6.948	332	205	−135.469	2.945	6.798	333	191
^{22}Mg	−168.246	1.063	3.298	465	242	−168.277	1.048	3.313	463	238
^{24}Mg	−196.822	1.058	3.438	470	233	−197.064	0.927	3.203	477	234
^{26}Mg	−215.322	1.679	4.725	283	151	−215.737	1.569	4.541	353	197
^{28}Mg	−231.242	1.527	4.080	291	167	−231.445	1.331	3.819	313	177
^{30}Mg	−243.563	1.882	4.760	257	154	−243.637	1.721	4.416	277	174
^{32}Mg	−253.381	2.270	4.283	122	212	−253.390	1.907	3.844	136	229
^{34}Mg	−260.198	1.050	2.842	367	214	−260.375	0.920	2.612	397	233
^{36}Mg	−266.045	0.679	2.024	460	238	−266.477	0.673	2.112	465	239
^{38}Mg	−269.022	0.785	2.286	487	261	−269.974	0.628	2.010	491	253
^{40}Mg	−271.098	0.556	1.815	502	261	−271.442	0.533	1.836	509	269

effect is strongest in ^{26}Mg, in which the 3DAMP+GCM yields an enhancement of ≈25% for the $B(E2;0_1^+ \rightarrow 2_1^+)$. Even in the triaxial case, the functional PC-F1 preserves the spherical shell closure at $N = 20$ (i.e., it predicts a spherical ground state for ^{32}Mg). The excitation energies of the states 2_1^+ and 4_1^+ in this nucleus are lowered considerably with respect to the axial case, but they are still much higher than the experimental values. Correspondingly, the calculated $B(E2;0_1^+ \rightarrow 2_1^+)$ is about a factor three smaller than the empirical value. It is noted, however, that when the pairing strength parameters are adjusted specifically to the empirical pairing gaps around ^{32}Mg, the calculated transition rate increases to $B(E2;0_1^+ \rightarrow 2_1^+) = 330.1$ e^{2}fm^4, much closer to the available data.

In future studies, the 3DAMP+GCM model based on relativistic density functionals will be applied to the description of shape transitions and shape coexistence phenomena in medium-heavy and heavy nuclei. We also plan to compare the results of full 3D angular-momentum projection and GCM configuration mixing, with those obtained in the recently developed model for the solution of the eigenvalue problem of a five-dimensional collective Hamiltonian for quadrupole vibrational and rotational degrees of freedom, with parameters determined by constrained self-consistent relativistic mean-field calculations for triaxial shapes [43].

ACKNOWLEDGMENTS

J.M.Y. would like to thank T. Nikšić for helpful discussions. This work was partly supported by the Major State 973 Program 2007CB815000 and the NSFC under Grants No. 10947013, No. 10975008, and No. 10775004, the Fundamental Research Funds for the Central Universities (XDJK2010B007), the Southwest University Initial Research Foundation Grant to Doctor (SWU109011), the DFG cluster of excellence "Origin and Structure of the Universe" (www.universe-cluster.de), by MZOS—project 1191005-1010, and by the Chinese-Croatian project "Nuclear structure far from stability."

APPENDIX: APPROXIMATE CORRECTION SCHEME FOR THE PARTICLE NUMBER

To approximately restore the correct mean value of the nucleon number in a GCM calculation, one usually subtracts two constraining terms for the average number of protons and neutrons [33,34]:

$$\mathcal{H}'(\boldsymbol{r};q,q';\Omega) = \mathcal{H}(\boldsymbol{r};q,q';\Omega) - \lambda_p[Z(\boldsymbol{r};q,q';\Omega) - Z_0] - \lambda_n[N(\boldsymbol{r};q,q';\Omega) - N_0], \quad \text{(A1)}$$

from the transition energy functional $\mathcal{H}(\boldsymbol{r};q,q';\Omega)$ as shown in Eq. (20) of Ref. [1]. Z_0 and N_0 are the desired proton and neutron numbers, respectively. $Z(\boldsymbol{r};q,q';\Omega)$ and $N(\boldsymbol{r};q,q';\Omega)$ are the transition vector densities in $\boldsymbol{r}$ space for protons and neutrons, respectively. In GCM calculations without angular-momentum projection that were considered in Ref. [34], the value of $\lambda_{\tau=p,n}$ was chosen to be the mean BCS Fermi energy, determined by averaging over the collective variable q. It was verified that the average particle numbers in the resulting GCM states differ only slightly from the desired values. However, it is not obvious that the quality of this correction scheme persists also in calculations with angular-momentum projection. In this appendix we examine the validity of this particle-number correction scheme by comparing results obtained in calculations without and with number correction, as well as those of exact particle-number projection for ^{24}Mg.

In practical calculations the λ_τ values in the transition-density energy functional correspond to the mean-field values [i.e., $\lambda_\tau(q)$ for the diagonal terms ($q' = q$), and $[\lambda_\tau(q) + \lambda_\tau(q')]/2$ for the off-diagonal terms ($q' \neq q$)]. To be able to compare with exact particle-number projection, the geometry is here restricted to the axially symmetric case, and 1DAMP+GCM calculations for ^{24}Mg are carried out with the PC-F1 effective interaction. The set of generator coordinates β is chosen: $\beta = -1.0, -0.9, \ldots, 1.1, 1.2$. The resulting $E2$ transition strength $B(E2;0_1^+ \rightarrow 2_1^+) = 471.5$ e^{2}fm^4 is very close to the value 469.6 e^{2}fm^4 (cf. Table I) obtained from the same model calculation but with fewer generator coordinates.

In Fig. 12 we display the mean-field and angular-momentum projected potential energy curves of ^{24}Mg, calculated without (left panel) and with (right panel) particle-number correction. One might notice that, without particle-number correction in certain regions of deformation, the projected PEC of 0^+ can even be found at excitation energies above those of 2^+, 4^+, and 6^+. Figure 13 displays the Fermi energies λ_τ, the pairing energies E_p of neutrons and protons in the intrinsic deformed states, and the corresponding average particle numbers $\langle \hat{N}_\tau \rangle$ in the angular-momentum projected states, as functions of the deformation parameter β. One notices that the deviation of the average particle number (mean value) from the desired number can be as large as 0.4 particles, both for neutron and protons. Moreover, this deviation displays a pronounced dependence on both the angular momentum J and deformation β. This simply follows from vector decomposition, as a weighed sum over all components has to yield the unprojected particle number. Therefore, the correction is different for each J component. The evident violation of the

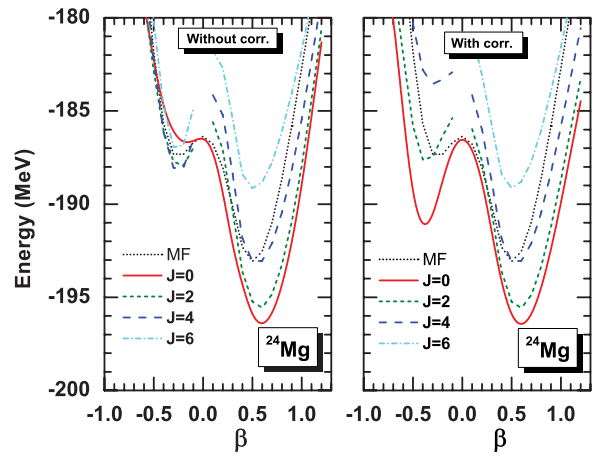

FIG. 12. (Color online) Mean-field and angular-momentum projected potential energy curves of ^{24}Mg calculated without (left panel) and with (right panel) particle-number correction.

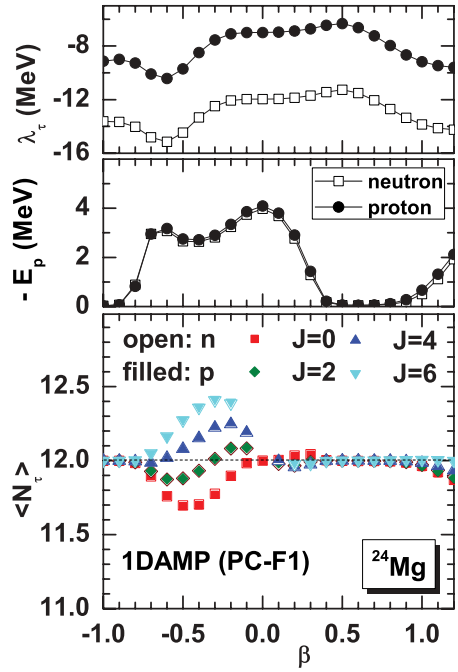

FIG. 13. (Color online) Fermi energies λ_τ and pairing energies E_p of neutrons (empty squares) and protons (filled circles) in the intrinsic deformed states, and the corresponding average particle numbers $\langle \hat{N}_\tau \rangle$ in the angular-momentum projected states, are plotted as functions of the deformation parameter β for ^{24}Mg.

desired particle number occurs for oblate deformations, for which pairing correlations are relatively large and the contribution from particle-number correction terms to the projected energy is significant. Having to correct for 0.4 missing or additional neutrons (protons) when the Fermi energy is about -12 MeV (-8 MeV), one obtains a correction of the order of 5 MeV (3 MeV), which is much larger than the spacing between energy levels that results from angular-momentum decomposition. This means that, when two levels J and J' differ by 0.4 in the average number of particles (cf. Fig. 13 for $J = 0$ and $J = 6$), the correction contributes about 8 MeV to the energy difference between these two levels, and this is of the same order as the energy difference from angular-momentum projection. The effect of the wrong average particle number on the uncorrected energies is so large that the usual ordering of levels might be inverted (cf. oblate shapes in Fig. 12). With the correction scheme described above, the ordering of angular-momentum projected PECs become normal, as shown in the right panel of Fig. 12.

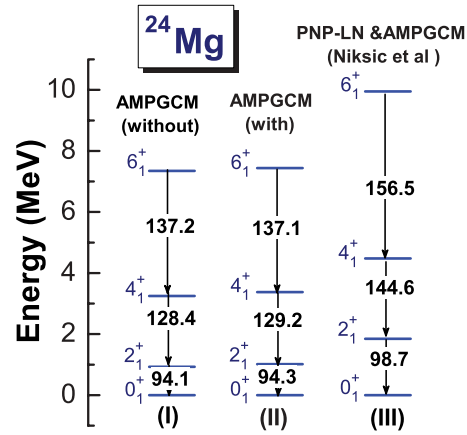

FIG. 14. (Color online) Yrast sequence of ^{24}Mg calculated in the 1DAMP+GCM model without (I) and with (II) the particle-number correction. In column III, the results obtained with an exact particle-number projection [31] are shown.

The energy spectrum of low-lying states in ^{24}Mg obtained from the 1DAMP+GCM calculations without and with the particle-number correction is displayed in Fig. 14, in comparison with the corresponding results of an exact particle-number projection (PNP) from Ref. [31]. We notice that the effect of particle-number correction on the low-spin yrast states is negligible. This is because the corresponding collective wave functions are concentrated on the prolate side, as shown in Fig. 9. With the Lipkin-Nogami (LN) approximate PNP before variation, and exact PNP after variation, the yrast sequence is more stretched as the LN avoids the collapse of pairing correlations in the prolate well. In addition, the corresponding $BE2$ values are larger by $\sim$10% in the PNP-LN calculation.

In summary, the correction for the particle number can be significant for some regions of deformation and is crucial for a proper description of angular-momentum projected energy curves. When compared with the results of calculations performed with an exact PNP after variation, in the case of axial symmetry the present model predicts a yrast energy spectrum that is more compressed because of pairing collapse, and the corresponding $B(E2)$ values are underestimated by $\sim$10%. As an important improvement of our current 3DAMP+GCM model, particle-number projection before and after variation need to be implemented to avoid pairing collapse and to yield the correct number of particles for each AMP+GCM state. However, one can expect to be confronted with the problems of discontinuities and divergences in the energy kernels [2,44–47].

[1] J. M. Yao, J. Meng, P. Ring, and D. Vretenar, Phys. Rev. C **81**, 044311 (2010).
[2] D. Lacroix, T. Duguet, and M. Bender, Phys. Rev. C **79**, 044318 (2009).
[3] M. Bender and P.-H. Heenen, Phys. Rev. C **78**, 024309 (2008).
[4] T. R. Rodriguez and J. L. Egido, Phys. Rev. C **81**, 064323 (2010).
[5] O. Sorlin and M.-G. Porquet, Prog. Part. Nucl. Phys. **61**, 602 (2008).
[6] T. Motobayashi *et al.*, Phys. Lett. B **346**, 9 (1995).
[7] D. Guillemaud-Mueller *et al.*, Nucl. Phys. A **426**, 37 (1984).
[8] H. Iwasaki *et al.*, Phys. Lett. B **522**, 227 (2001).
[9] S. Takeuchi *et al.*, Phys. Rev. C **79**, 054319 (2009).
[10] B. V. Pritychenko *et al.*, Phys. Lett. B **461**, 322 (1999).

[11] J. M. Cook, T. Glasmacher, and A. Gade, Phys. Rev. C **73**, 024315 (2006).
[12] A. Gade *et al.*, Phys. Rev. Lett. **99**, 072502 (2007).
[13] A. Gade *et al.*, Phys. Rev. C **76**, 024317 (2007).
[14] V. Chisé *et al.*, Phys. Lett. B **514**, 233 (2001).
[15] O. Niedermaier *et al.*, Phys. Rev. Lett. **94**, 172501 (2005).
[16] W. Schwerdtfeger *et al.*, Phys. Rev. Lett. **103**, 012501 (2009).
[17] E. Caurier, F. Nowacki, A. Poves, and J. Retamosa, Phys. Rev. C **58**, 2033 (1998).
[18] Y. Utsuno, T. Otsuka, T. Mizusaki, and M. Honma, Phys. Rev. C **60**, 054315 (1999).
[19] T. Otsuka, R. Fujimoto, Y. Utsuno, B. A. Brown, M. Honma, and T. Mizusaki, Phys. Rev. Lett. **87**, 082502 (2001).
[20] T. Otsuka, Y. Utsuno, T. Mizusaki, and M. Honma, Nucl. Phys. A **685**, 100 (2001).
[21] E. Caurier, G. Martiez-Pinedo, F. Nowacki, A. Poves, and A. P. Zuker, Rev. Mod. Phys. **77**, 427 (2005).
[22] F. Maréchal *et al.*, Phys. Rev. C **72**, 044314 (2005).
[23] J. Terasaki, H. Flocarda, P. H. Heenen, and P. Bonche, Nucl. Phys. A **621**, 706 (1997).
[24] R. Rodríguez-Guzmán, J. L. Egido, and L. M. Robledo, Nucl. Phys. A **709**, 201 (2002).
[25] S. K. Patra and C. R. Praharaj, Phys. Lett. B **273**, 13 (1991).
[26] Z. Z. Ren, Z. Y. Zhu, Y. H. Cai, and G. Xu, Phys. Lett. B **380**, 241 (1996).
[27] Q. J. Zhi and Z. Z. Ren, Phys. Lett. B **638**, 166 (2006).
[28] A. Valor, P. H. Heenen, and P. Bonche, Nucl. Phys. A **671**, 145 (2000).
[29] M. Bender, P.-H. Heenen, and P.-G. Reinhard, Rev. Mod. Phys. **75**, 121 (2003).
[30] T. Nikšić, D. Vretenar, and P. Ring, Phys. Rev. C **73**, 034308 (2006).
[31] T. Nikšić, D. Vretenar, and P. Ring, Phys. Rev. C **74**, 064309 (2006).
[32] J. M. Yao, J. Meng, P. Ring, and D. Pena Arteaga, Phys. Rev. C **79**, 044312 (2009).
[33] K. Hara, A. Hayashi, and P. Ring, Nucl. Phys. A **385**, 14 (1982).
[34] P. Bonche, J. Dobaczewski, H. Flocard, P.-H. Heenen, and J. Meyer, Nucl. Phys. A **510**, 466 (1990).
[35] T. Burvenich, D. G. Madland, J. A. Maruhn, and P. G. Reinhard, Phys. Rev. C **65**, 044308 (2002).
[36] J. L. Egido, L. M. Robledo, and Y. Sun, Nucl. Phys. A **560**, 253 (1993).
[37] L. M. Robledo, Phys. Rev. C **50**, 2874 (1994).
[38] S. Raman, C. W. Nestor Jr., and P. Tikkanen, At. Data Nucl. Data Tables **78**, 1 (2001).
[39] M. Bender, G. F. Bertsch, and P. H. Heenen, Phys. Rev. C **73**, 034322 (2006).
[40] P. Ring and P. Schuck, *The Nuclear Many-Body Problem* (Springer-Verlag, New York, 1980).
[41] S. Raman, C. W. Nestor, and K. H. Bhatt, Phys. Rev. C **37**, 805 (1988).
[42] N. Imai *et al.*, Phys. Rev. Lett. **92**, 062501 (2004).
[43] T. Nikšić, Z. P. Li, D. Vretenar, L. Próchniak, J. Meng, and P. Ring, Phys. Rev. C **79**, 034303 (2009).
[44] M. Anguiano, J. L. Egido, and L. M. Robledo, Nucl. Phys. A **696**, 467 (2001).
[45] J. Dobaczewski, M. V. Stoitsov, W. Nazarewicz, and P.-G. Reinhard, Phys. Rev. C **76**, 054315 (2007).
[46] M. Bender, T. Duguet, and D. Lacroix, Phys. Rev. C **79**, 044319 (2009).
[47] T. Duguet, M. Bender, K. Bennaceur, D. Lacroix, and T. Lesinski, Phys. Rev. C **79**, 044320 (2009).